arXiv:hep-th/0701288v2 3 May 2007

hep-th/0701288

Greybody Factors for Brane Scalar Fields in a Rotating Black-Hole Background

S. Creek[1], **O. Efthimiou**[2], **P. Kanti**[1,2] and **K. Tamvakis**[2]

[1] *Department of Mathematical Sciences, University of Durham, Science Site, South Road, Durham DH1 3LE, United Kingdom*

[2] *Division of Theoretical Physics, Department of Physics, University of Ioannina, Ioannina GR-45110, Greece*

Abstract

We study the evaporation of $(4+n)$-dimensional rotating black holes into scalar degrees of freedom on the brane. We calculate the corresponding absorption probabilities and cross-sections obtaining analytic solutions in the low-energy regime, and compare the derived analytic expressions to numerical results, with very good agreement. We then consider the high-energy regime, construct an analytic high-energy solution to the scalar-field equation by employing a new method, and calculate the absorption probability and cross-section for this energy regime, finding again a very good agreement with the exact numerical results. We also determine the high-energy asymptotic value of the total cross-section, and compare it to the analytic results derived from the application of the geometrical optics limit.

1 Introduction

Among the motivations for consideration of higher-dimensional theories [1, 2] is that the leading candidates (String Theory and variants of it), for the unification of gravity with the rest of the fundamental interactions at the quantum level, are all formulated in a higher-dimensional context. In these models, gravity propagates in $D = 4+n$ dimensions (*Bulk*), while matter degrees of freedom are confined to live on a 4-dimensional hypersurface (*Brane*). In models with large extra dimensions [1], the traditional Planck scale $M_{Pl} \sim 10^{18}\, GeV$ is only an effective scale, related to the fundamental higher-dimensional gravity scale M_* through the relation $M_{Pl}^2 \sim M_*^{n+2} R^n$, where $R \sim (V_n)^{1/n}$ is the effective size of the n extra spatial dimensions. If $R \gg \ell_{Pl} \approx 10^{-33}\, cm$, the scale M_* can be substantially lower than M_{Pl}. In that case, trans-planckian particle collisions could probe the strong-gravity regime and possibly produce higher-dimensional black holes [3] centered at the brane and extending in the bulk. For all the classical laws of black-hole physics to still hold, the mass of the black hole M_{BH} would have to be larger than M_*. Nevertheless, the properties of these higher-dimensional black holes would still be modified compared to their 4-dimensional analogues [4, 5].

If M_* is sufficiently low, such black holes may be produced in ground-based colliders [6], although their appearance in cosmic rays is possible as well [7] (for reviews, see [5, 8, 9]). A black hole created in such trans-planckian collisions is expected to gradually lose its angular momentum and finally its mass through the emission of Hawking radiation [10], consisting of elementary particles of a characteristic thermal spectrum, both in the bulk and on the brane. The emitted radiation from a higher-dimensional black hole created in trans-planckian collisions has been studied both analytically and numerically. Until recently, the *Schwarzschild* phase, along with a variety of additional spherically-symmetric black-hole backgrounds, were the most commonly studied cases. Those studies included the black-hole emission of lower-spin degrees of freedom [11, 12, 13, 14, 15, 16, 17, 18] as well as gravitons [19, 20, 21, 22], both on the brane and in the bulk.

The complexity of the gravitational background around an axially-symmetric black hole, increased by the presence of extra dimensions, deterred many researchers from investigating the radiation spectrum of a higher-dimensional rotating black hole. However, during the last two years, a plethora of studies of the Hawking radiation, emitted by such a black hole, appeared in the literature [23, 24, 25, 26, 27, 28, 29, 30]. These works offered exact numerical results that supplemented and generalized two early analytic works focussed on the particular case of a 5-dimensional rotating black hole [31, 32]. Nevertheless, to our knowledge, up to now no work has performed a complete analytic study of the emission of Hawking radiation from a rotating black hole in an arbitrary number of dimensions.

In the present article, we consider the evaporation of a $(4 + n)$-dimensional rotating black hole into scalar degrees of freedom on the brane. We calculate the corresponding absorption probabilities and cross-sections obtaining analytical solutions in both the high and low-energy regimes. In section 2, we consider the metric corresponding to a higher-dimensional rotating black hole, and write down the equation for scalar fields propagating in the projected-on-the-brane background. In section 3, we focus on the low-energy

regime, and solve analytically the scalar-field equation employing the *matching technique* of combining the far-field and near-horizon parts of the solution. Subsequently, we derive an analytic expression for the absorption probability, and produce a set of plots exhibiting its dependence on particle quantum numbers and topological properties of spacetime. We proceed by deriving corresponding numerical plots, and compare them to the analytic ones, with excellent agreement. We finally derive a low-energy, simplified expression for the absorption cross-section, and confirm the universal behaviour characterising the absorption of scalar fields in this particular energy regime. In section 4, we turn our attention to the high-energy regime. We construct an analytic high-energy solution to the scalar-field equation by employing a new method involving *Kummer functions*, and calculate the absorption probability at this energy regime. By using our analytic results, we produce plots which we compare to the corresponding numerical ones finding again a very good agreement. In the same section, we determine, through numerical integration, the exact asymptotic value of the total absorption cross-section at the high-energy regime. We also include an analytic treatment of the *geometrical optics limit*, which is expected to correspond to the high-energy asymptotic regime. We derive expressions for the absorption cross-section in this limit for three distinct kinematical cases, and compare them with the exact numerical results. Finally, in section 5, we state our conclusions.

2 Gravitational Background and Field Equations

If one accepts the prospect of the creation of a microscopic black hole during a high-energy particle collision, then, due to a generically non-vanishing value of the impact parameter between the two particles, the emergence of a rotating black hole is the most natural outcome. As the black hole is created in the framework of the higher-dimensional theory, that is characterized by a strong gravitational force, it will itself be a higher-dimensional object, that "feels" the extra compact, spacelike dimensions. Under the assumption that the black-hole horizon r_h is significantly smaller than the size of the extra dimensions, the spacetime around it may be approximated by one with a single timelike dimension and $(3+n)$ non-compact, spacelike ones. A black hole living in such a background can have in general up to $[(n+3)/2]$ angular momentum parameters. However, here, we will be assuming that the colliding particles are restricted to propagate on an infinitely-thin 3-brane, therefore, they will have a non-zero impact parameter only along our brane, and thus acquire only one non-zero angular momentum parameter about an axis in the brane. The background around a higher-dimensional rotating black hole with one angular momentum parameter is given by the following Myers-Perry solution [33]

$$ds^2 = \left(1 - \frac{\mu}{\Sigma\, r^{n-1}}\right) dt^2 + \frac{2a\mu \sin^2\theta}{\Sigma\, r^{n-1}}\, dt\, d\varphi - \frac{\Sigma}{\Delta}\, dr^2 - \Sigma\, d\theta^2$$
$$- \left(r^2 + a^2 + \frac{a^2 \mu \sin^2\theta}{\Sigma\, r^{n-1}}\right) \sin^2\theta\, d\varphi^2 - r^2 \cos^2\theta\, d\Omega_n^2, \qquad (1)$$

where

$$\Delta = r^2 + a^2 - \frac{\mu}{r^{n-1}}\,, \qquad \Sigma = r^2 + a^2\, \cos^2\theta\,, \qquad (2)$$

and $d\Omega_n^2$ is the line-element on a unit n-sphere. The mass and angular momentum of the black hole are then given by

$$M_{BH} = \frac{(n+2)A_{n+2}}{16\pi G}\,\mu\,, \qquad J = \frac{2}{n+2}\,M_{BH}\,a\,, \tag{3}$$

with G being the $(4+n)$-dimensional Newton's constant, and A_{n+2} the area of a $(n+2)$-dimensional unit sphere given by

$$A_{n+2} = \frac{2\pi^{(n+3)/2}}{\Gamma[(n+3)/2]}\,. \tag{4}$$

Since the creation of the black hole depends crucially on the value of the impact parameter between the two highly-energetic particles [3], and that in turn defines the angular momentum of the black hole, an upper bound can be imposed on the angular momentum parameter a of the black hole by demanding the creation of the black hole itself during the collision. The maximum value of the impact parameter between the two particles that can lead to the creation of a black hole is [9]

$$b_{\rm max} = 2\left[1+\left(\frac{n+2}{2}\right)^2\right]^{-\frac{1}{(n+1)}}\mu^{\frac{1}{(n+1)}}\,, \tag{5}$$

an analytic expression that is in very good agreement with the numerical results produced in the third paper of Ref. [3]. If we write $J = bM_{BH}/2$, for the angular momentum of the black hole, and use the following expression for the black-hole horizon

$$r_h^{n+1} = \frac{\mu}{1+a_*^2}\,, \tag{6}$$

that follows from the equation $\Delta(r) = 0$, and the second of Eqs. (3), we obtain

$$a_*^{\rm max} = \frac{n+2}{2}\,. \tag{7}$$

In the above, we have defined, for convenience, the quantity $a_* = a/r_h$. Equation (7), thus, puts an upper bound to the value of the black-hole angular momentum parameter, which for $n > 1$ would have been unrestricted, contrary to the cases of $n = 0$ and $n = 1$, where a maximum value of a exists that guarantees the existence of a real solution for the black-hole horizon.

In this work, we will focus on the propagation of scalar fields in the gravitational background induced on the brane, where all ordinary particles are assumed to live. The 4-dimensional induced background will be the projection of the higher-dimensional one onto the brane, and its exact expression follows by fixing the values of the additional azimuthal angular variables – introduced to describe the n compact extra dimensions – to $\theta_i = \pi/2$, for $i = 2, ..., n+1$. Then, the induced-on-the-brane line-element takes the form

$$\begin{aligned} ds^2 = \left(1-\frac{\mu}{\Sigma\, r^{n-1}}\right)dt^2 + \frac{2a\mu\sin^2\theta}{\Sigma\, r^{n-1}}\,dt\,d\varphi - \frac{\Sigma}{\Delta}dr^2 \\ - \Sigma\, d\theta^2 - \left(r^2+a^2+\frac{a^2\mu\sin^2\theta}{\Sigma\, r^{n-1}}\right)\sin^2\theta\, d\varphi^2\,. \end{aligned} \tag{8}$$

Note that although the above background is very similar to the usual 4-dimensional Kerr one, it is not exactly the same due to its explicit dependence on the number of additional spacelike dimensions n. It is this dependence that will cause brane quantities to depend on the number of dimensions that exist transverse to the brane.

In order to study the propagation of fields in the above background, we need to derive first their equations of motion. We assume that the particles couple only minimally to the gravitational background and have no other interactions, therefore, they satisfy the corresponding free equations of motion. The latter, for particles with spin 0, 1/2 and 1, propagating in the induced-on-the-brane gravitational background (8), were derived in [5, 32]. For scalar fields, the field factorization

$$\phi(t, r, \theta, \varphi) = e^{-i\omega t}\, e^{im\varphi}\, R_{\omega\ell m}(r)\, T_\ell^m(\theta, a\omega)\,, \tag{9}$$

where $T_\ell^m(\theta, a\omega)$ are the so-called spheroidal harmonics [34], was shown to lead to the following set of decoupled radial and angular equations

$$\frac{d}{dr}\left(\Delta\, \frac{dR_{\omega\ell m}}{dr}\right) + \left(\frac{K^2}{\Delta} - \Lambda_\ell^m\right) R_{\omega\ell m} = 0\,, \tag{10}$$

$$\frac{1}{\sin\theta}\frac{d}{d\theta}\left(\sin\theta\, \frac{dT_\ell^m(\theta, a\omega)}{d\theta}\right) + \left(-\frac{m^2}{\sin^2\theta} + a^2\omega^2\cos^2\theta + E_\ell^m\right) T_\ell^m(\theta, a\omega) = 0\,, \tag{11}$$

respectively. In the above, we have defined

$$K = (r^2 + a^2)\,\omega - am\,, \qquad \Lambda_\ell^m = E_\ell^m + a^2\omega^2 - 2am\omega\,. \tag{12}$$

The angular eigenvalue $E_\ell^m(a\omega)$ provides a link between the angular and radial equation. Its expression, in general, cannot be written in closed form, however, an analytic form can be found [35] in terms of a power series with respect to the parameter $a\omega$. We will return to this point in Section 3.

By solving Eq. (10), we determine the radial part of the field wavefunction, and, subsequently, the absorption probability $|\mathcal{A}_{\ell,m}|^2$ for the propagation of a scalar field in the projected-on-the-brane background. This quantity appears in the differential emission rates for Hawking radiation emitted by the higher-dimensional black hole on the brane. For example, the particle flux, i.e. the number of particles emitted per unit time and unit frequency, has the form

$$\frac{d^2N}{dtd\omega} = \frac{1}{2\pi}\sum_{\ell,m}\frac{1}{\exp\left[k/T_{\rm H}\right] - 1}|\mathcal{A}_{\ell,m}|^2\,; \tag{13}$$

similar formulae may be written for the energy and angular momentum emission rates. In the above, k and T_H stand for

$$k \equiv \omega - m\Omega = \omega - \frac{ma}{r_h^2 + a^2}\,, \qquad T_{\rm H} = \frac{(n+1) + (n-1)a_*^2}{4\pi(1 + a_*^2)r_h}\,, \tag{14}$$

with Ω the angular velocity of the black hole and T_H its temperature. The absorption probability $|\mathcal{A}_{\ell,m}|^2$ depends both on particle properties (energy ω, angular momentum

numbers ℓ, m, etc) and gravitational background properties (number of extra dimensions n, black-hole angular momentum parameter a). As a result, it modifies the various emission rates from the ones for a blackbody. Equation (10) has been solved analytically only for the case of a 5-dimensional rotating black hole (and then, only in the low-energy regime) [32], and numerically in [23, 25, 27] for arbitrary dimensions[1]. In the next sections, we will attempt to derive analytic results, both in the low- and high-energy regimes, for the absorption probability for scalar fields propagating in the 4-dimensional spacetime of a brane embedded in the background of a rotating black hole of arbitrary dimensionality.

3 Greybody Factor in the Low-Energy Regime

In this section, we focus on the solution for the absorption probability in the low-energy regime. We will first derive an analytic expression by using a well-known approximate method. We will then plot this expression to reveal its dependence on a number of parameters, such as the angular momentum numbers of the particle, the dimensionality of spacetime, and the angular momentum of the black hole. It will also be directly compared with the exact numerical results derived earlier in the literature. We will finally derive a compact analytic expression, valid in the limit $\omega \to 0$, and comment on the form of the corresponding absorption cross-section and its relation to the area of the black-hole horizon.

3.1 Solving the Field Equation Analytically

In what follows, we will use an approximate method and solve first the radial equation of motion (10) at the two asymptotic regimes: close to the black-hole horizon ($r \simeq r_h$), and far away from it ($r \gg r_h$). The two solutions will then be stretched and matched in an intermediate zone to create a smooth analytical solution extending over the whole radial regime.

We first focus on the near-horizon regime and make the following change of variable

$$r \to f(r) = \frac{\Delta(r)}{r^2 + a^2} \implies \frac{df}{dr} = (1-f)\, r\, \frac{A(r)}{r^2 + a^2}\,, \tag{15}$$

where, for convenience, we have defined the function $A(r) \equiv (n+1) + (n-1)\, a^2/r^2$. Then, Eq. (10), near the horizon ($r \simeq r_h$), takes the form

$$f\,(1-f)\,\frac{d^2P}{df^2} + (1 - D_*\, f)\,\frac{dP}{df} + \left[\, \frac{K_*^2}{A_*^2\, f(1-f)} - \frac{\Lambda_\ell^m\,(1+a_*^2)}{A_*^2\,(1-f)} \,\right] P = 0\,, \tag{16}$$

where now

$$A_* = (n+1) + (n-1)\, a_*^2\,, \qquad K_* = (1+a_*^2)\,\omega_* - a_* m\,, \tag{17}$$

[1]The angular equation (11) was also solved numerically in [25], and the angular distribution of the emitted radiation was found.

with $\omega_* \equiv \omega r_h$. We have also defined the quantity

$$D_* \equiv 1 + \frac{n\,(1+a_*^2)}{A_*} - \frac{4a_*^2}{A_*^2}\,. \tag{18}$$

By making the field redefinition $P(f) = f^\alpha (1-f)^\beta F(f)$, Eq. (16) takes the form of a hypergeometric equation [36]:

$$f\,(1-f)\,\frac{d^2F}{df^2} + [c - (1+a+b)\,f]\,\frac{dF}{df} - ab\,F = 0\,, \tag{19}$$

with

$$a = \alpha + \beta + D_* - 1\,, \qquad b = \alpha + \beta\,, \qquad c = 1 + 2\alpha\,. \tag{20}$$

The power coefficients α and β will be determined by two constraints (following from the demand that the coefficient of $F(f)$ is indeed $-ab$) that have the form of second-order algebraic equations, namely

$$\alpha^2 + \frac{K_*^2}{A_*^2} = 0\,, \tag{21}$$

and

$$\beta^2 + \beta\,(D_* - 2) + \frac{K_*^2}{A_*^2} - \frac{\Lambda_\ell^m\,(1+a_*^2)}{A_*^2} = 0\,. \tag{22}$$

The general solution of the hypergeometric equation (19), combined with the relation between $P(f)$ and $F(f)$, leads to the following expression for the radial function $P(f)$ in the near-horizon regime:

$$\begin{aligned} P_{NH}(f) = {} & A_-\, f^\alpha\,(1-f)^\beta\,F(a,b,c;f) \\ & + A_+\, f^{-\alpha}\,(1-f)^\beta\,F(a-c+1,b-c+1,2-c;f)\,, \end{aligned} \tag{23}$$

where $A_\pm$ are arbitrary constants. Solving Eq. (21), we obtain the solutions

$$\alpha_\pm = \pm\frac{iK_*}{A_*}\,. \tag{24}$$

Near the horizon, $r \to r_h$ and $f(r) \to 0$. Then, the near-horizon solution (23) reduces to

$$P_{NH}(f) \simeq A_-\, f^{\pm iK_*/A_*} + A_+\, f^{\mp iK_*/A_*} = A_-\, e^{\pm iky} + A_+\, e^{\mp iky}\,, \tag{25}$$

where, in the second part, we have used the definition for k given in Eq. (14), and the tortoise-like coordinate $y = r_h(1+a_*^2)\ln(f)/A_*$. Note, that although the coordinate y is not identical to the usual tortoise-one, defined by $dr_*/dr = (r^2+a^2)/\Delta(r)$, used in Kerr-like backgrounds [37], it holds that

$$\frac{dy}{dr} = \left(\frac{A}{A_*}\right)\,\frac{(r_h^2+a^2)^2}{(r^2+a^2)^2}\,\left(\frac{r_h}{r}\right)^{n-2}\,\frac{dr_*}{dr}\,. \tag{26}$$

Therefore, in the limit $r \to r_h$, the two become identical, and the near-horizon asymptotic solution assumes, as expected, the free-wave form in terms of the tortoise-coordinate

[23, 25, 37]. Imposing the boundary condition that no outgoing mode exists near the horizon, we are forced to set either $A_- = 0$ or $A_+ = 0$, depending on the choice for α. As the two are clearly equivalent, we choose $\alpha = \alpha_-$, and set $A_+ = 0$. This brings our near-horizon solution to the final form

$$P_{NH}(f) = A_- f^{\alpha} (1-f)^{\beta} F(a,b,c;f) \,. \tag{27}$$

We finally turn to Eq. (22) for the β power coefficient. This admits the solutions

$$\beta_{\pm} = \frac{1}{2} \left[(2 - D_*) \pm \sqrt{(D_* - 2)^2 - \frac{4K_*^2}{A_*^2} + \frac{4\Lambda_\ell^m (1+a_*^2)}{A_*^2}} \right] . \tag{28}$$

The sign appearing in front of the square root will be decided by the criterion for the convergence of the hypergeometric function $F(a,b,c;f)$, i.e. $\mathrm{Re}\,(c-a-b) > 0$, which demands that we choose $\beta = \beta_-$.

We now turn our attention to the far-field regime. Making the assumption that $r \gg r_h$, and keeping only the dominant terms in the expansion in terms of $1/r$, the radial equation (10) takes the form

$$\frac{d^2P}{dr^2} + \frac{2}{r}\frac{dP}{dr} + \left(\omega^2 - \frac{E_l^m + a^2\omega^2}{r^2} \right) P(r) = 0 \,, \tag{29}$$

where E_l^m is the angular eigenvalue. The substitution $P(r) = \frac{1}{\sqrt{r}} \tilde{P}(r)$ brings the above into the form of a Bessel equation for $\tilde{P}(r)$, and the overall solution in the far-field limit can be written as

$$P_{FF}(r) = \frac{B_1}{\sqrt{r}} J_\nu (\omega r) + \frac{B_2}{\sqrt{r}} Y_\nu (\omega r) \,, \tag{30}$$

where J_ν and Y_ν are the Bessel functions of the first and second kind, respectively, with $\nu = \sqrt{E_l^m + a^2\omega^2 + 1/4}$, and $B_{1,2}$ integration constants.

In order to construct an analytic solution extending over the whole radial regime, we need to smoothly match the two asymptotic solutions, derived above, in some intermediate regime. Before doing so, we first need to extrapolate (stretch) the two solutions towards this regime. To this end, we shift the argument of the hypergeometric function of the near-horizon solution from f to $1-f$ by using the relation [36]

$$\begin{aligned} P_{NH}(f) &= A_- f^{\alpha} (1-f)^{\beta} \left[\frac{\Gamma(c)\,\Gamma(c-a-b)}{\Gamma(c-a)\,\Gamma(c-b)} F(a,b,a+b-c+1;1-f) \right. \\ &+ \left. (1-f)^{c-a-b} \frac{\Gamma(c)\,\Gamma(a+b-c)}{\Gamma(a)\,\Gamma(b)} F(c-a,c-b,c-a-b+1;1-f) \right] . \end{aligned} \tag{31}$$

The function $f(r)$ may be alternatively written as

$$f(r) = 1 - \frac{\mu}{r^{n-1}} \frac{1}{r^2 + a^2} = 1 - \left(\frac{r_h}{r} \right)^{n-1} \frac{(1+a_*^2)}{(r/r_h)^2 + a_*^2} \,, \tag{32}$$

where we have used the horizon equation, $\Delta(r_h) = 0$, in order to eliminate μ from the above relation. In the limit $r \gg r_h$, the $(r/r_h)^2$ in the denominator of the second term above is dominant, and the whole expression goes to unity for $n \geq 0$. Thus, in the limit $f \to 1$, the near-horizon solution (31) takes the form

$$P_{NH}(r) \simeq A_1\, r^{\,-(n+1)\,\beta} + A_2\, r^{\,(n+1)\,(\beta+D_*-2)}\,, \tag{33}$$

with

$$\begin{aligned} A_1 &= A_-\left[(1+a_*^2)\, r_h^{n+1}\right]^{\beta}\, \frac{\Gamma(c)\Gamma(c-a-b)}{\Gamma(c-a)\Gamma(c-b)} \\ A_2 &= A_-\left[(1+a_*^2)\, r_h^{n+1}\right]^{-(\beta+D_*-2)}\, \frac{\Gamma(c)\Gamma(a+b-c)}{\Gamma(a)\Gamma(b)}\,. \end{aligned} \tag{34}$$

Next we need to stretch the far-field asymptotic solution (30) towards small values of the radial coordinate. Then, in the limit $\omega r \to 0$, we find

$$\begin{aligned} P_{FF}(r) \simeq & \frac{B_1\left(\frac{\omega r}{2}\right)^{\sqrt{E_l^m+a^2\omega^2+1/4}}}{\sqrt{r}\,\Gamma\left(\sqrt{E_l^m+a^2\omega^2+1/4}+1\right)} \\ & - \frac{B_2}{\pi\sqrt{r}}\,\Gamma\left(\sqrt{E_l^m+a^2\omega^2+1/4}\right)\left(\frac{\omega r}{2}\right)^{-\sqrt{E_l^m+a^2\omega^2+1/4}}\,. \end{aligned} \tag{35}$$

We notice that both 'stretched' asymptotic solutions have reduced to power-law expressions in terms of the radial coordinate r, however, the different power coefficients prevent the exact matching. In order to overcome this obstacle, we will expand these power coefficients in the limits $(\omega r_h)^2 \ll 1$ and $(a/r_h)^2 \ll 1$. It is these approximations that will limit the validity of our result for the absorption probability to the low-energy and low-angular-momentum regime. Note, however, that in order to improve the accuracy of our result, no approximation will be made in the arguments of the Gamma functions involved in Eqs. (33) and (35). In order to follow the aforementioned line of action, we need to know the analytic expression for the angular eigenvalue E_l^m. According to [35], this may be written as a power series in terms of the parameter $(a\omega)$, namely

$$E_l^m = \sum_{n=0}^{\infty} f_n^{lm}\,(a\omega)^n\,. \tag{36}$$

For the purposes of our analysis, we have calculated the coefficients f_n^{lm} up to fifth order, and found the result

$$\begin{aligned} E_l^m &= l\,(l+1) + (a\omega)^2\,\frac{[2m^2-2l\,(l+1)+1]}{(2l-1)\,(2l+3)} \\ &+ (a\omega)^4\,\left\{\frac{2\,[-3+17l\,(l+1)+l^2(l+1)^2(2l-3)\,(2l+5)]}{(2l-3)\,(2l+5)\,(2l+3)^3(2l-1)^3}\right. \\ &+ \frac{4m^2}{(2l-1)^2(2l+3)^2}\,\left[\frac{1}{(2l-1)\,(2l+3)} - \frac{3l\,(l+1)}{(2l-3)\,(2l+5)}\right] \\ &+ \left.\frac{2m^4\,[48+5(2l-1)\,(2l+3)]}{(2l-3)\,(2l+5)\,(2l-1)^3(2l+3)^3}\right\} + ...\,, \end{aligned} \tag{37}$$

with $f_1^{lm} = f_3^{lm} = f_5^{lm} = 0$. The above form will be used at every place where E_l^m appears in Eqs. (33) and (35). The only exception will be in the power coefficients, where terms of order $(a\omega)^2$, or higher, will be ignored. Following these assumptions, the two power coefficients in Eq. (33) reduce to

$$\begin{aligned} -(n+1)\,\beta &\simeq l + \mathcal{O}(\omega_*^2, a_*^2, a_*\omega_*)\,, \\ (n+1)\,(\beta + D_* - 2) &\simeq -(l+1) + \mathcal{O}(\omega_*^2, a_*^2, a_*\omega_*)\,. \end{aligned} \tag{38}$$

while the power coefficient in Eq. (35) takes the form

$$\sqrt{E_l^m + a^2\omega^2 + 1/4} \simeq \left(l + \frac{1}{2}\right) + \mathcal{O}(a_*^2\omega_*^2)\,. \tag{39}$$

By using the above results, one can easily show that both Eqs. (33) and (35) reduce to power-law expressions with the same power coefficients, r^l and $r^{-(l+1)}$. By matching the corresponding coefficients, we determine the integration constants $B_{1,2}$ in terms of the other parameters of the theory. Their ratio, which, as we shall see, appears in the expression of the absorption probability $|\mathcal{A}_{l,m}|^2$, is found to be

$$\begin{aligned} B \equiv \frac{B_1}{B_2} = -\frac{1}{\pi}\left(\frac{2}{\omega r_h\,(1+a_*^2)^{\frac{1}{n+1}}}\right)^{2l+1} \sqrt{E_l^m + a^2\omega^2 + 1/4} \\ \times \frac{\Gamma^2\left(\sqrt{E_l^m + a^2\omega^2 + 1/4}\right)\Gamma(\alpha+\beta+D_*-1)\,\Gamma(\alpha+\beta)\,\Gamma(2-2\beta-D_*)}{\Gamma(2\beta+D_*-2)\,\Gamma(2+\alpha-\beta-D_*)\,\Gamma(1+\alpha-\beta)}\,. \end{aligned} \tag{40}$$

The last step in our calculation of the absorption probability involves the expansion of the far-field solution (30) to infinity ($r \to \infty$). This leads to

$$\begin{aligned} P_{FF}(r) &\simeq \frac{1}{\sqrt{2\pi\omega}}\left[\frac{(B_1 + iB_2)}{r}\,e^{-i\left(\omega r - \frac{\pi}{2}\,\nu - \frac{\pi}{4}\right)} + \frac{(B_1 - iB_2)}{r}\,e^{i\left(\omega r - \frac{\pi}{2}\,\nu - \frac{\pi}{4}\right)}\right] \\ &= A_{in}^{(\infty)}\,\frac{e^{-i\omega r}}{r} + A_{out}^{(\infty)}\,\frac{e^{i\omega r}}{r}\,. \end{aligned} \tag{41}$$

As expected, at large distances from the black hole, where the effect of the angular momentum parameter a is almost negligible, the solution for the scalar field reduces to a spherical wave, as in the Schwarzschild case [11, 23, 25]. Then, the absorption probability is defined through the expression

$$\begin{aligned} |\mathcal{A}_{l,m}|^2 &= 1 - \left|\frac{A_{out}^{(\infty)}}{A_{in}^{(\infty)}}\right|^2 = 1 - \left|\frac{B_1 - iB_2}{B_1 + iB_2}\right|^2 \\ &= 1 - \left|\frac{B - i}{B + i}\right|^2 = \frac{2i\,(B^* - B)}{BB^* + i\,(B^* - B) + 1}\,. \end{aligned} \tag{42}$$

The above result, together with the expression for B given in Eq. (40), is our main analytic result for the absorption probability for scalar fields valid in the low-energy and low-angular-momentum regime. It can be easily checked that it reduces smoothly to the corresponding result for a scalar field propagating in a Schwarzschild-like, higher-dimensional background projected onto the brane [11], if we set $a = 0$.

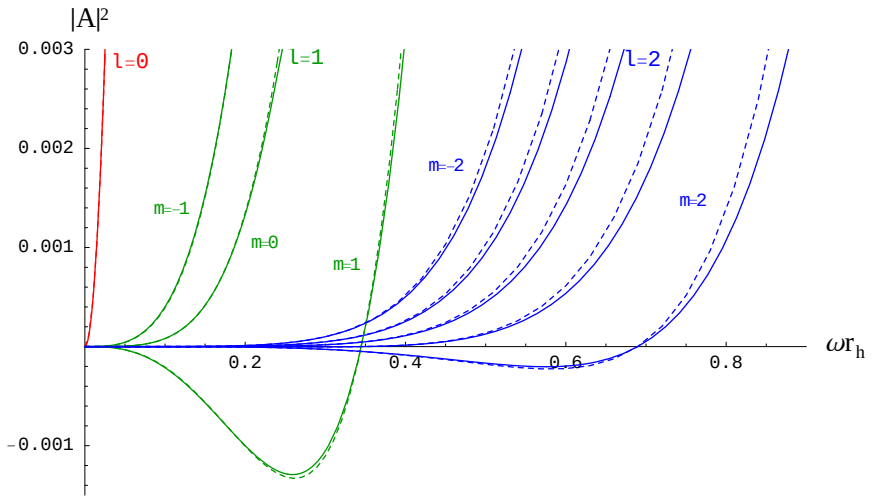

Figure 1: Absorption probability $|\mathcal{A}_{l,m}|^2$ for brane scalar particles, for $n = 2$, $a_* = 0.4$, and for the modes (from left to right) $(l = m = 0)$, $(l = 1, m = -1, 0, 1)$, and $(l = 2, m = -2, -1, 0, 1, 2)$. The solid lines correspond to our analytic results, and the dashed lines to the exact numerical ones.

3.2 A Comparison with the Exact Numerical Solution

In this section, we proceed to study in detail the properties of the absorption probability $|\mathcal{A}_{l,m}|^2$, as this was derived above by using purely analytic arguments. To this end, we will plot our main result, given by Eqs. (42) and (40), as a function of the energy parameter ωr_h and for a variety of values of the other parameters of the theory, namely the angular momentum numbers (l, m) of the scalar particle, and the topological parameters (a_*, n) of the spacetime. At the same time, a direct comparison of our low-energy analytic result to the exact numerical value for $|\mathcal{A}_{l,m}|^2$ – derived in [9, 23, 25] for the purpose of computing the Hawking radiation emission spectra – will be performed in order to examine the range of validity of our approximations.

In Fig. 1, we plot the absorption probability $|\mathcal{A}_{l,m}|^2$ for scalar particles, for fixed angular momentum of the black hole ($a_* = 0.4$) and number of extra dimensions ($n = 2$), and for a variety of modes with different angular momentum numbers (l, m). Throughout our paper, our analytic results will be plotted by using solid lines while the exact numerical results, reproduced from [9, 23, 25], will be denoted by dashed lines. In Fig. 1, both sets of lines are shown for all modes, and the agreement between them at low energy is indeed remarkable. Although a small deviation appears when the energy parameter is taken beyond the low-energy regime, the qualitative agreement between the two sets of results remains excellent.

Focusing now on the dependence of the absorption probability on particle parameters, we observe that, similarly to the Schwarzschild case [11], it is again the lowest partial wave, with $l = 0$, that dominates in the low-energy regime, with all higher modes increasingly suppressed. This behaviour is valid for all values of a_* and n, as long as attention is focused on the low-energy regime. Looking next at the relative behaviour of

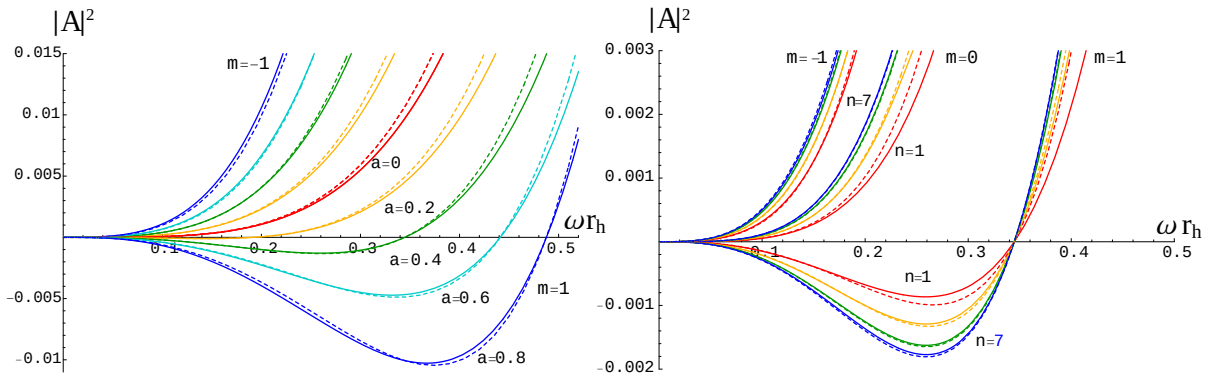

Figure 2: Absorption probability $|\mathcal{A}_{l,m}|^2$ for brane scalar particles, **(a)** for the modes $(l = 1, m = -1, 1)$, for $n = 2$ and $a_* = (0, 0.2, 0.4, 0.6, 0.8)$, and **(b)** for the modes $(l = 1, m = -1, 0, 1)$, for $a_* = 0.4$ and $n = (1, 2, 4, 7)$. Again, the solid lines correspond to our analytic results, and the dashed lines to the exact numerical ones.

modes with the same angular momentum number l but different number m, we easily note that the modes with $m < 0$ are the dominant ones with increasing m causing suppression. We also observe that, for modes with $m \leq 0$, the absorption probability always remains positive, while, for modes with $m > 0$, a negative-valued region for $|\mathcal{A}_{l,m}|^2$ always appears in the low-energy regime. The latter effect is due to the so-called superradiance [38] – the enhancement of the amplitude of an incoming wave by a rotating black hole that results in a reflection probability larger than unity, and thus a negative absorption probability according to $|\mathcal{A}_{l,m}|^2 = 1 - |\mathcal{R}_{l,m}|^2$. We will say a little more on the origin of this effect in the following subsection.

We now turn to the dependence of the absorption probability on the parameters of spacetime. In Fig. 2, we depict the behaviour of $|\mathcal{A}_{l,m}|^2$ in terms of the angular momentum parameter a_* and number of extra dimensions n. We have chosen the indicative case of $l = 1$, and, in Fig. 2(a), depict the behaviour of the $m = -1$ (from central to left) and $m = 1$ (from central to right) modes, for a range of values of a_*. Then, in Fig. 2(b), we present all three modes, with $m = 0, \pm 1$, for various values of n. As before, both the analytic, low-energy results as well as the exact numerical ones are shown. Again, the agreement between the two sets of results in the low-energy regime is remarkably good. The alert reader may note that, in general, the agreement between the two sets is improving as n increases: this is due to the fact that, according to Eq. (32), an increase in the number of extra dimensions improves the accuracy of the assumed behaviour of the function $f(r)$ at infinity, and consequently our approximation. In addition, terms that have been neglected during the matching of the two asymptotic solutions under the low-energy and low-a_* assumption, such as the K_*^2/A_*^2 in Eq. (28), become even smaller for large values of n, thus improving the accuracy of our analysis.

According to Fig. 2(a), for fixed n, the non-superradiant modes, with $m \leq 0$ (although not shown, the $m = 0$ mode exhibits a behaviour similar to the $m = -1$), are enhanced with the angular momentum of the black hole in the low-energy regime, while the superradiant modes, with $m > 0$, are suppressed both in the superradiant and non-

superradiant energy regime. Turning to Fig. 2(b), we note that, for fixed a_*, an increase in the number of extra dimensions n also leads to an enhancement of the value of the absorption probability for the non-superradiant modes. For the superradiant ones, the behaviour of $|\mathcal{A}_{l,m}|^2$ depends on the energy regime we are looking at: while it is suppressed in the superradiant regime, it is enhanced in the non-superradiant one. From both figures, it becomes obvious that the superradiant effect becomes more important as either a_* or n increases. This enhancement, for brane-localised scalar particles, both in terms of the angular momentum of the black hole and the dimensionality of spacetime was also noted in the literature [23, 24, 28].

3.3 The Low-Energy Asymptotic Limit of the Cross-Section

Our last task regarding the behaviour of the absorption probability $|\mathcal{A}_{l,m}|^2$ in the low-energy regime will be the derivation, from Eqs. (40) and (42), of a compact analytic expression valid in the limit $\omega \to 0$. This simplified analytic expression will be used to explain some of the features discussed in the previous subsection. In addition, from this, the asymptotic low-energy value of the corresponding absorption cross-section for scalar fields in the background of a projected-on-the-brane rotating black hole will also be determined.

We start our analysis by noticing that, according to Eq. (40), in the limit $\omega \to 0$, $B \sim \omega^{-(2l+1)}$ and, therefore, $BB^* \gg i(B^* - B) \gg 1$. Then, Eq. (42) simplifies to

$$|\mathcal{A}_{l,m}|^2 \simeq \frac{2i(B^* - B)}{BB^*} = 2i\left(\frac{1}{B} - \frac{1}{B^*}\right) . \tag{43}$$

Substituting for B using Eq. (40), and the fact that α is purely imaginary, yields

$$\begin{aligned} |\mathcal{A}_{l,m}|^2 \;=\; & \frac{-2i\pi\,(\omega r_h/2)^{2l+1}}{(l+\frac{1}{2})\,\Gamma^2(l+\frac{1}{2})}\frac{\Gamma(2\beta+D_*-2)}{(1+a_*^2)^{-\frac{2l+1}{n+1}}\,\Gamma(2-2\beta-D_*)} \quad \times \\ & \frac{1}{\Gamma(\alpha+\beta+D_*-1)\,\Gamma(-\alpha+\beta+D_*-1)\,\Gamma(\alpha+\beta)\,\Gamma(-\alpha+\beta)} \quad \times \\ & \Big[\Gamma(2+\alpha-\beta-D_*)\,\Gamma(-\alpha+\beta+D_*-1)\,\Gamma(1+\alpha-\beta)\,\Gamma(-\alpha+\beta) - \\ & \Gamma(2-\alpha-\beta-D_*)\,\Gamma(\alpha+\beta+D_*-1)\,\Gamma(1-\alpha-\beta)\,\Gamma(\alpha+\beta)\Big] \qquad (44) \\ =\; & \Sigma_1 \times \Sigma_2 \times \Sigma_3 \,, \end{aligned}$$

where Σ_1, Σ_2 and Σ_3 are defined by the quantities on each of the three lines above. Focusing first our attention to Σ_3, and using the Gamma function relation $\Gamma(z)\Gamma(1-z) = \pi/\sin\pi z$ [36], this can be written as

$$\Sigma_3 = \frac{-\pi^2\,\sin(2\pi\alpha)\,\sin\pi(2\beta+D_*)}{\sin\pi(\alpha+\beta+D_*)\,\sin\pi(-\alpha+\beta+D_*)\,\sin\pi(\alpha+\beta)\,\sin\pi(-\alpha+\beta)} . \tag{45}$$

From the factor ω^{2l+1} in Eq. (44), it becomes clear that the expression for the absorption probability at the very low-energy regime is dominated by the lowest partial waves, a

property that is in accordance with the results presented in the previous subsection. Then, assuming that m is small and $a_* < 1$, the limit $\omega \to 0$ is equivalent to $\alpha \to 0$. Expanding terms in Σ_3 and Σ_2 to linear order in α gives

$$\Sigma_3 = -\frac{2\pi^3 \alpha \, \sin\pi(2\beta + D_*)}{\sin^2\pi(\beta + D_*)\, \sin^2\pi\beta}\,, \qquad \Sigma_2 = \frac{1}{\Gamma(\beta + D_* - 1)^2\, \Gamma(\beta)^2}\,. \tag{46}$$

Using the additional Gamma function relation $\Gamma(z)\Gamma(-z) = -\pi/z\sin\pi z$ allows the overall expression for the low-energy limit of the absorption probability to be written as

$$|\mathcal{A}_{l,m}|^2 = \frac{4\pi\,(\omega r_h/2)^{2l+1}\, K_*\, \sin^2\pi(2\beta + D_*)\, \Gamma^2(2\beta + D_* - 2)\, \Gamma^2(1-\beta)\, (2 - D_* - 2\beta)}{A_*\, (1 + a_*^2)^{-\frac{2l+1}{n+1}}\, (l + \frac{1}{2})\, \Gamma^2(l + \frac{1}{2})\, \Gamma^2(\beta + D_* - 1)\, \sin^2\pi(\beta + D_*)}\,. \tag{47}$$

In the above, we have also used the definition $\alpha \equiv -iK_*/A_*$, where, from Eq. (17),

$$K_* = (1 + a_*^2)\,\omega_* - a_*\, m = r_h(1 + a_*^2)\,(\omega - m\,\Omega)\,. \tag{48}$$

By using Eq. (28), one may easily conclude that the quantity $(2 - D_* - 2\beta)$ is always positive, while the same also holds for $A_* \equiv (n+1) + (n-1)a_*^2$, for all values for a_* and $n > 0$. Therefore, the overall sign of $|\mathcal{A}_{l,m}|^2$ is determined by the sign of K_*, or equivalently of $(\omega - m\,\Omega)$. A negative sign for the latter combination arises only for $m > 0$, and denotes the occurrence of superradiance, with $|\mathcal{A}_{l,m}|^2$ acquiring a negative value. The superradiance domain arises in the low-energy regime and extends over the range of values $0 < \omega < \omega_s \equiv m\,\Omega$. The larger the value of the angular momentum parameter a_*, the larger the rotation velocity Ω of the black hole, and thus the more extended the superradiance regime becomes. This is indeed in agreement with the behaviour found in the previous subsection.

In what follows, we focus on the dominant s-wave with $l = m = 0$. As we will see, this will be the only partial wave with a non-vanishing low-energy asymptotic value of the absorption cross-section. In order to simplify further Eq. (47), we need also to expand the expression of β in the limit $\omega \to 0$. It is easy to see that, in this limit, $\beta = 0 + \mathcal{O}(\omega^2)$, which then allows us to write

$$|\mathcal{A}_0|^2 = \frac{4\,(\omega r_h)^2\,(1 + a_*^2)}{A_*\,(1 + a_*^2)^{-1/(n+1)}\,(2 - D_*)} + \dots\,. \tag{49}$$

The corresponding absorption cross-section for the dominant partial wave is then given by [39]

$$\sigma_0 = \frac{\pi}{\omega^2}\,|\mathcal{A}_0|^2 = 4\pi\,(r_h^2 + a^2)\,\frac{(1 + a_*^2)^{1/(n+1)}}{[(n+1) + (n-1)\,a_*^2]\,(2 - D_*)} + \dots\,. \tag{50}$$

According to the above result, the absorption cross-section for the lowest mode $l = 0$ reduces to a non-vanishing asymptotic value, as $\omega \to 0$. We may easily see, from Eq. (47), that the low-energy behaviour of the absorption probability for any higher partial mode will be governed by the factor ω^{2l+2}, thus leading to an absorption cross-section proportional to ω^{2l}. Therefore, for all partial waves with $l \neq 0$, the partial cross-section goes to zero, as $\omega \to 0$.

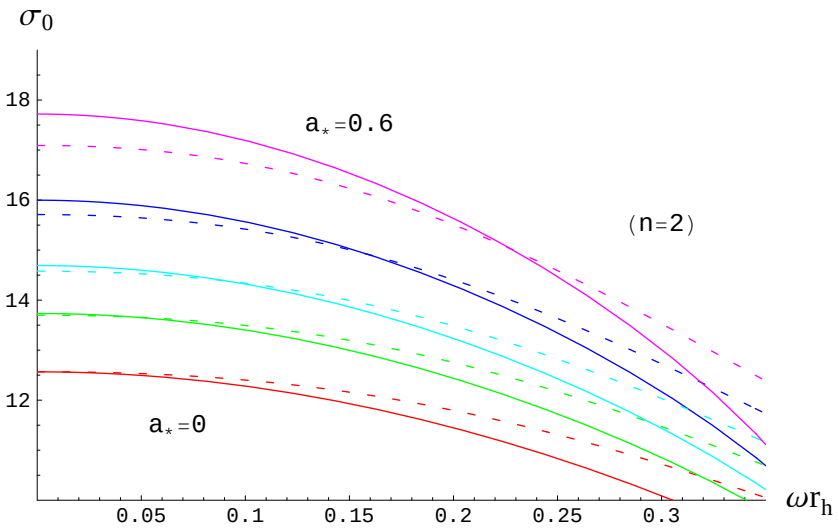

Figure 3: Absorption cross-section σ_0 (in units of r_h^2) for the lowest scalar mode $l = 0$, for $n = 2$ and a_* ranging between 0 and 0.6. As before, the solid lines correspond to our analytic results, and the dashed lines to the exact numerical ones.

In the case of scalar particles propagating in a Schwarzschild-like projected-on-the-brane line-element, the low-energy asymptotic value of the absorption cross-section of the lowest, dominant partial wave was shown to be equal to the horizon area of the 4-dimensional black hole, $4\pi r_h^2$, regardless of the number of extra dimensions [11, 13]. We would like to demonstrate that a similar relation holds in the case of an axially-symmetric brane background. According to Eq. (50), σ_0 is indeed proportional to the horizon area of the four-dimensional rotating black hole $4\pi(r_h^2 + a^2)$, however, the relation involves a multiplicative factor which is both (a_*, n)-dependent. In Fig. 3, we plot σ_0, for fixed n and various values of a_*, by using both our analytic expression and the exact numerical result. The latter set of results reveal that the asymptotic low-energy cross-section is indeed equal to the horizon area of the black hole, regardless of the number of extra dimensions. For small values of a_*, the multiplicative factor appearing in Eq. (50) is very close to unity and our analytic expression closely reproduces the exact numerical one. As a_* increases though, the range of validity of our approximation is exceeded and a deviation starts appearing, as expected. If we keep a_* fixed and vary n instead, a similar behaviour appears, with values of $n \leq 1$ leading, in general, to a value smaller than the exact result, and values of $n \geq 2$ to a value larger than the exact result. The magnitude of the deviation depends again on the value of a_*. The above results demonstrate the universal behaviour for the lowest partial mode of a scalar particle according to which its partial cross-section equals the area of the black-hole horizon in the low-energy regime. This result holds not only for a spherically-symmetric brane line-element but also for an axially-symmetric one, and is independent of the number of the transverse-to-the-brane spacelike dimensions. The latter result was also reproduced for the particular case of a 5-dimensional bulk in [30].

4 Greybody Factor in the High-Energy Regime

In this section, we turn our attention to the high-energy regime, and present a way to compute the absorption probability in this region by using again the matching technique described in section 3. For this, we are going to use the near-horizon solution we have already computed in Section 3.1, and we shall construct an approximate, high-energy, far-field solution that will allow us to do the matching solely in the high-energy regime. Next, we are going to compare the absorption coefficient produced this way with the exact numerical results of the literature. Finally, generalizing well-known results for Schwarzschild black holes, the geometrical optics limit value of the absorption cross-section will be computed, and its connection to the high-energy asymptotic value found by numerical analysis will be investigated.

4.1 Analytic Construction of the Solution

In order to construct a solution over the whole radial domain that will be valid in the high-energy regime, it is necessary to do the matching of the stretched near-horizon and far-field asymptotic solutions without resorting to the low-energy approximation ($\omega r_h \ll 1$) employed in section 3.1. To this end, we will try to find a new far-field asymptotic solution that will satisfy the field equation only in the high-energy limit. Moreover, the exact form of this solution should be such that, when stretched towards small values of the radial coordinate, it reduces to a power-law expression with identical power coefficients to the ones appearing in the stretched near-horizon solution, thus allowing for a perfect matching in the intermediate regime. We remind the reader that the stretched near-horizon solution, (Eq. 33), was found to be of the form

$$P_{NH} \simeq A_1\, r^{\,-(n+1)\beta} + \mathrm{A}_2\, r^{\,(n+1)(\beta+D_*-2)} \equiv A_1\, r^{\,\beta_1} + A_2\, r^{\,\beta_2}\,. \tag{51}$$

The differential equation that our far-field solution needs to satisfy is Eq. (10) in the limit $r \gg r_h$, or equivalently

$$\frac{d^2P_{FF}}{dz^2} + \frac{2z}{z^2+a_1^2}\,\frac{dP_{FF}}{dz} + \left(1 - \frac{E_l^m + a_1^2}{z^2+a_1^2}\right) P_{FF}(z) = 0\,, \tag{52}$$

where we have made the change of variable $z = \omega r$, and defined for convenience $a_1 = a\omega$. Let us consider the following trial, special solution to the above equation

$$P_{FF} = e^{-i\omega r} r^{\,\beta_1} M\left(1+\beta_1, 2+2\beta_1; 2i\omega r\right)\,, \tag{53}$$

where $M(\hat{a},\hat{b};w)$ is the first Kummer function [36]. Solving Eq. (53) for $M(\hat{a},\hat{b};w)$ and substituting in the confluent hypergeometric equation, that the Kummer functions satisfy,

$$\frac{d^2M}{dw^2} + (\hat{b}-w)\,\frac{dM}{dw} - \hat{a}\,M(w) = 0\,, \tag{54}$$

with $\hat{a} = 1+\beta_1$, $\hat{b} = 2+2\beta_1$ and $w = 2i\omega r$, we finally obtain the equation

$$\frac{d^2P_{FF}}{dz^2} + \frac{2}{z}\,\frac{dP_{FF}}{dz} + \left(1 - \frac{\beta_1\,(\beta_1+1)}{z^2}\right) P_{FF} = 0\,. \tag{55}$$

Subtracting Eq. (55) from Eq. (52), we find

$$2\,\frac{dP_{FF}}{dz}\left(\frac{z}{z^2+a_1^2}-\frac{1}{z}\right)+P_{FF}\left(\frac{\beta_1(\beta_1+1)}{z^2}-\frac{E_\ell^m+a_1^2}{z^2+a_1^2}\right)=0+\mathcal{O}(1/z^2)\,.$$

From the above, we may conclude that, for large $z=\omega r$, the constructed solution (53) satisfies the far-field ($r\gg r_h$) equation (52) up to second order in $(1/z)$. Therefore, in the limit $\omega\to\infty$, our trial solution (53) is indeed a good approximation to the exact solution of the field equation in the far-field regime.

By following the same method, a second special solution to Eq. (52) may be constructed that has the form

$$P_{FF}=e^{-i\omega r}\,r^{\,-\beta_2-1}\,U\left(-\beta_2,-2\beta_2;2i\omega r\right)\,, \tag{56}$$

where $U(\hat{a},\hat{b};w)$ is the second Kummer function. The second special solution follows from the first one under the replacement $\beta_1\to-1-\beta_2$, which preserves the structure of Eq. (55). Therefore, this solution, too, is a good approximation to the exact solution of Eq. (52) in the limit $\omega\to\infty$. Therefore, the total solution in the far-field domain, valid only in the high-energy regime, takes the form

$$P_{FF}=B_+\,e^{-i\omega r}r^{\,\beta_1}M(\beta_1+1,2\beta_1+2,2i\omega r)+B_-\,e^{-i\omega r}r^{\,-\beta_2-1}\,U(-\beta_2,-2\beta_2,2i\omega r)\,. \tag{57}$$

The Kummer functions have been used before in the construction of the far-field solution of a general spin-s field [5, 11], however, the projected-on-the-brane background in that case was that of a spherically-symmetric Schwarzschild-like one. We may easily check that, in the limit $a\to 0$, the above solution reduces to the one for a scalar field propagating in the far-field domain of a spherically-symmetric brane black-hole background.

As an additional independent check of the above analysis, one may observe that, under the demand that Eq. (55) matches exactly Eq. (52), we are led to

$$\beta_1=-\frac{1}{2}+\sqrt{E_l^m+a^2\omega^2+1/4}=-\frac{1}{2}+\nu\,. \tag{58}$$

But then, since $\hat{a}=\nu+1/2$ and $\hat{b}=2\nu+1$, the first Kummer function reduces to $M(\nu+1/2,2\nu+1;2i\omega r)\sim e^{i\omega r}\,r^{-\nu}J_\nu(\omega r)$ [36]. By using this result – as well as a similar one for the second Kummer function U – in conjunction with the relations (53) and (56), we may see that the far-field solution (30), found in section 3.1, is duly restored as expected.

Nevertheless, in this section, the approximate solution (57) will be used instead, since, as was mentioned earlier, its use will allow us to achieve a perfect matching between the stretched near-horizon and far-field solutions – a feature that, as we saw, was not possible when the asymptotic solution (30) was used instead. To this end, we stretch Eq. (57) to small values of ωr [36] to obtain

$$P_{FF}=B_+\,r^{\,\beta_1}+\mathrm{B}_-\,r^{\,\beta_2}\,\frac{\Gamma(-2\beta_2-1)}{\Gamma(-\beta_2)}\,(2i\omega)^{2\beta_2+1}\,. \tag{59}$$

As we hoped, the stretched far-field solution contains powers of r that exactly match the ones appearing in the stretched near-horizon solution (51). Then, by matching also the corresponding multiplicative coefficients, we find

$$\tilde{B} \equiv \frac{B_-}{B_+} = \frac{\left[(1+a_*^2)\, r_h^{n+1}\right]^{2-2\beta-D_*}}{(2i\omega)^{2\beta_2+1}} \times \frac{\Gamma(2\beta+D_*-2)\,\Gamma(2+\alpha-\beta-D_*)\,\Gamma(1+\alpha-\beta)\,\Gamma(-\beta_2)}{\Gamma(\alpha+\beta+D_*-1)\,\Gamma(\alpha+\beta)\,\Gamma(2-2\beta-D_*)\,\Gamma(-2\beta_2-1)}\,. \quad (60)$$

We remind the reader that the coefficients D_*, α and β are given in Eqs. (18), (24) and (28), respectively, while the coefficients $\beta_{1,2}$ are defined in Eq. (51).

In order to finally compute the absorption probability, we need first to expand the far-field solution (57) in the limit $r \to \infty$. Then, we find [36]

$$\begin{aligned} P_{FF} &\simeq \frac{e^{-i\omega r}}{r}\left[B_+\,\frac{\Gamma(2+2\beta_1)}{\Gamma(1+\beta_1)}\,\frac{e^{i\pi(\beta_1+1)}}{(2i\omega)^{\beta_1+1}} + B_-\,(2i\omega)^{\beta_2}\right] + \frac{e^{i\omega r}}{r}\frac{B_+\,\Gamma(2+2\beta_1)}{\Gamma(1+\beta_1)\,(2i\omega)^{\beta_1+1}} + ... \\ &\equiv A_{in}^{(\infty)}\,\frac{e^{-i\omega r}}{r} + A_{out}^{(\infty)}\,\frac{e^{i\omega r}}{r}\,. \end{aligned} \quad (61)$$

As we see, the far-field solution (57) also reduces to a spherical free-wave solution in the asymptotic infinity. We may thus use once again the standard definition for the absorption probability to determine its value

$$|\mathcal{A}_{l,m}|^2 = 1 - \left|\frac{A_{out}^{(\infty)}}{A_{in}^{(\infty)}}\right|^2 = 1 - \left|\frac{\Gamma(2+2\beta_1)}{\Gamma(2+2\beta_1)\,e^{i\pi(\beta_1+1)} + \tilde{B}\,\Gamma(\beta_1+1)\,(2i\omega)^{\beta_1+\beta_2+1}}\right|^2 . \quad (62)$$

The above expression, combined with Eq. (60), gives the absorption probability for scalar fields, valid only in the high-energy regime, but with no restrictions on the value of the angular momentum parameter a apart from the upper bound of Eq. (7). The corresponding absorption cross-section, valid in the high-energy regime, then follows by using the formula $\sigma_{l,m} = \pi|\mathcal{A}_{l,m}|^2/\omega^2$ and Eq. (62).

In Figs. 4(a,b), we depict the absorption probability $|\mathcal{A}_{l,m}|^2$ and cross-section $\sigma_{l,m}$, respectively, for brane scalar particles, in the high-energy regime. Once again, the solid lines correspond to our analytic results, following from Eq. (62), and the dashed lines to the exact numerical ones. Figure 4(a) depicts the absorption probability for the indicative case of the three lowest partial modes. We notice that our analytic results match the exact numerical ones for large enough value of the energy ω. The lower the value l of the partial mode, the sooner the two results coincide. As the energy parameter increases, the absorption probability quickly tends to unity – as expected, highly energetic particles always overcome the gravitational barrier outside the horizon of the black hole. This asymptotic behaviour, although successfully reproduced by our analytic results, does not allow us to appreciate the agreement between the two sets of results. For this reason, in Fig. 4(b), we plot the absorption cross-section for the three lowest partial waves summed over m: in the high-energy regime, $\sigma_{l,m} \sim 1/\omega^2$ for all modes, and the asymptotic regime is significantly more extended. The agreement between our analytic and numerical results

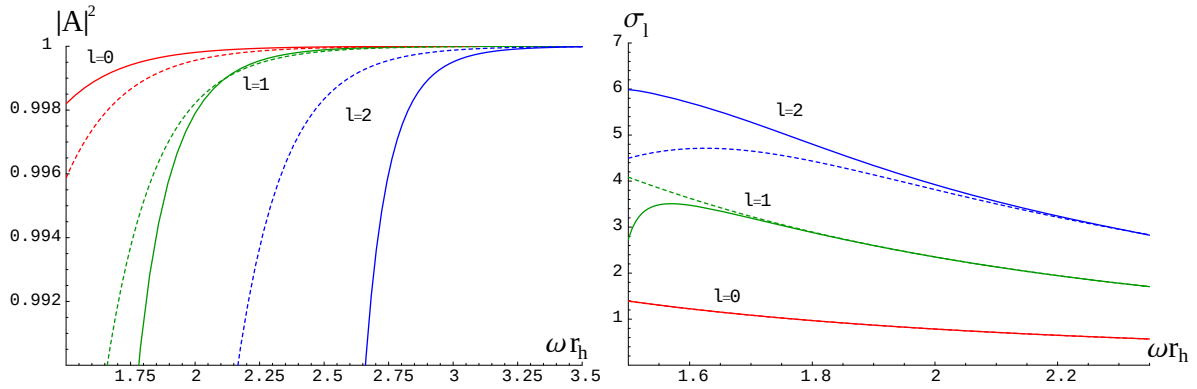

Figure 4: **(a)** Absorption probability $|\mathcal{A}_l|^2$ for brane scalar particles, for the modes $l = 0, 1, 2$ and $m = 0$, for $n = 2$ and $a_* = 0.3$, and **(b)** absorption cross-section σ_l (in units of r_h^2), for the modes $l = 0, 1, 2$ (summed over m), and for the same values of n and a_* as before. Again, the solid lines correspond to our analytic results, and the dashed lines to the exact numerical ones.

is now much clearer: for the mode $l = 0$, the two results completely coincide, while, for $l = 1, 2$, the exact matching is achieved at gradually larger values of energy. Once matched, the two results remain identical as ω increases further until the zero asymptotic value – for the individual partial modes – is reached. Given the increased difficulty in integrating numerically both the radial and angular part of the scalar equation of motion over an extended energy regime (for example, see [13, 25]), the above solution could be used to analytically extrapolate a numerical solution to arbitrarily large values of the energy parameter ω.

4.2 High-Energy Asymptotic and Geometrical Optics Limits

As the energy of the particle emitted from a black hole increases, the total absorption cross-section $\sigma_{\rm abs} = \sum_{l,m} \sigma_{l,m}$ reaches a high-energy asymptotic value, in an oscillatory way. Although each partial cross-section $\sigma_{l,m}$ asymptotes zero at the high-energy regime, the superposition of an infinite number of partial waves, each one reaching its maximum value at a gradually larger value of ω as l increases, creates this constant asymptotic value. This asymptotic limit has been studied in the past for a Schwarzschild black hole, both in the four-dimensional [40, 41, 42, 43] and $(4+n)$-dimensional case [13, 44]. For a rotating black hole, the corresponding study was performed in 4 dimensions in [45], and in 5 dimensions in [30].

Here, we will attempt to give a comprehensive study of the high-energy asymptotic limit of the total absorption cross-section for scalar fields living on the brane-induced line-element of a $(4+n)$-dimensional rotating black hole. As we will see, similarly to the case of a Schwarzschild-like induced-on-the-brane line-element, the number of transverse dimensions, although inaccessible to the brane-localised scalar fields, affects the value of the high-energy asymptotic limit of the absorption cross-section. The value of the angular momentum parameter a_* of the higher-dimensional black hole will also be found

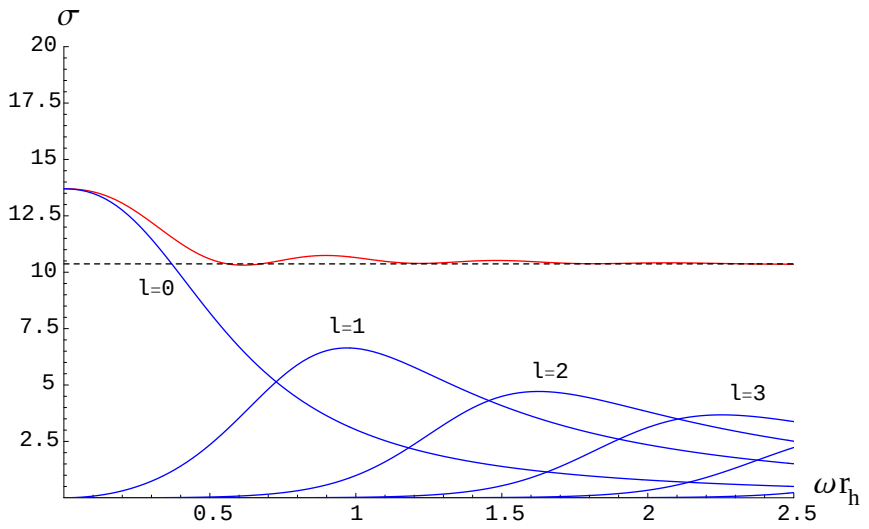

Figure 5: Partial absorption cross-sections σ_l, for the modes $l = 0, 1, 2, 3, 4$ (lower set of curves), and the total absorption cross-section $\sigma_{\rm abs}$ (upper curve) for $n = 2$ and $a_* = 0.3$, both in units of r_h^2. The dashed line denotes the value obtained by using the geometrical optics limit (69).

to have an effect on the value of $\sigma_{\rm abs}$. Although our analytic results describe successfully, as we saw in previous sections, both the low- and high-energy regimes of the absorption probability and cross-section, no analytic solution currently exists that smoothly connects the two solutions over the intermediate energy regime. The emergence of the high-energy asymptotic limit of the total absorption cross-section strongly relies on the contribution of the low-energy regime (where the $l = 0$ mode dominates), the intermediate-energy regime (where all modes have a significant contribution) and the high-energy regime (where higher modes dominate). As a result, in order to accurately derive the high-energy asymptotic value of $\sigma_{\rm abs}$, and in the absence of a global analytic solution, the use of exact numerical analysis is imperative.

In Fig. 5, we therefore present exact numerical results for the absorption cross-section $\sigma_l = \sum_m \sigma_{l,m}$ for the partial modes $l = 0, 1, 2, 3, 4$, as well as for the total absorption cross-section $\sigma_{\rm abs}$ for a brane-localised scalar field, for the indicative case of $n = 2$ and $a_* = 0.3$. The emergence of a constant high-energy asymptotic value for the total cross-section is obvious. In the context of our analysis, we have studied the behaviour of $\sigma_{\rm abs}$ for a range of values of n and a_*, with our results being displayed in Table 1. Note that, while for low values of n and a_*, a relatively small number of partial modes needs to be summed over (for the case depicted in Fig. 5, only modes up to $l = 5$ were included in the calculation), as either a_* or n takes large values, an increasing number of partial waves needs to be taken into account. In addition, as either a_* or n increases further, the asymptotic value of $\sigma_{\rm abs}$ emerges at continuously larger values of ω, which significantly increases the computing time.

From the entries of Table 1, one may observe the strong dependence of the high-energy asymptotic limit of the absorption cross-section on both the number of transverse-

$\mathbf{a_*\backslash n}$	1	2	3	4	5	6
0.0	12.6	9.6	8.2	7.3	6.7	6.2
0.3	13.6	10.4	8.6	7.6	7.0	6.5
0.5	15.7	11.5	9.5	8.4	7.6	7.1
0.7	18.7	13.2	10.7	9.4	8.5	7.9
1.0	25.1	16.6	13.2	11.4	10.3	9.5
1.5	40.7	24.1	18.6	15.8	14.0	12.9
2.0	62.8	33.6	25.2	21.1	18.7	17.2

Table 1: High-energy asymptotic values of the total absorption cross-section $\sigma_{\rm abs}$, in units of r_h^2, as a function of n and a_*.

to-the-brane dimensions and the angular momentum of the black hole. As in the non-rotating case [13], $\sigma_{\rm abs}$ is strongly suppressed as n increases. On the other hand, an increase in the value of a_* causes an enhancement in the value of $\sigma_{\rm abs}$. For $a_* = 0$, the values of $\sigma_{\rm abs}$ match, as expected, the ones obtained for a scalar particle in a Schwarzschild-like projected brane background [13]. We would also like to note that a feature that seemed to hold in the 5-dimensional case [30], namely that the high-energy asymptotic value of $\sigma_{\rm abs}$ is close to the low-energy one, disappears for general n. This can be clearly seen in Fig. 5, or by comparing the entries of Table 1 with the value of σ_0, from Eq. (50), that dominates the low-energy value of $\sigma_{\rm abs}$: for general n, the two sets of values are distinctly different.

In the case of a non-rotating black hole, the geometrical optics limit has been successfully used to explain the high-energy asymptotic value of the absorption cross-section $\sigma_{\rm abs}$ both in the pure 4-dimensional case [40, 41, 42, 43] and $(4+n)$-dimensional one [13, 44]. In the higher-dimensional case, for particles living on the brane, the geometrical optics analysis showed that the Schwarzschild black hole behaves as a perfect absorber of a radius given by

$$r_c = r_h \left(\frac{n+3}{2}\right)^{\frac{1}{n+1}} \sqrt{\frac{n+3}{n+1}}\,. \tag{63}$$

The absorption cross-section is then given by the target area, $\sigma_{\rm abs} = \pi r_c^2$. The values following from this expression, for different n, are in perfect agreement with the numerical ones found in [13], and displayed here in the first row of Table 1.

Here, we will attempt to perform a similar study, in an axially-symmetric black-hole brane background, and investigate the potential connection between the analytic values that follow from this analysis and the exact numerical ones depicted in Table 1, for $a_* \neq 0$. For this, we will closely follow the method described in [45]. Although that formalism was developed for the case of a pure 4-dimensional Kerr black hole, it holds identically for the case of a projected-on-the-brane rotating black hole, with the only difference appearing in the exact expression of the metric function $\Delta(r)$. We therefore present here only the basic assumptions and the final equation that describe the particle's trajectory.

The line-element (8), in which the brane-localised particles propagate, is invariant under translations of the form $t \to t + \Delta t$ and $\phi \to \phi + \Delta\phi$. The corresponding Killing vectors $\xi^{\mu}_{(t)} = \delta^{\mu}_{t}$ and $\xi^{\mu}_{(\varphi)} = \delta^{\mu}_{\varphi}$ then lead to the conserved conjugate momenta $p_t \equiv -E$ and $p_\phi \equiv -L_z$. The brane metric also possesses a Killing tensor $\xi_{\mu\nu}$, that leads to an additional conserved quantity $\mathcal{Q} = \xi_{\mu\nu}\, p^{\mu} p^{\nu} - (Ea + L_z)^2$. Combining the above, the equation of motion of a particle with rest mass m, i.e. $p_\mu\, p^\mu = m^2$, takes the form [45]

$$\Sigma \frac{dr}{d\lambda} = \pm \mathcal{R}^{1/2}\,, \quad \mathcal{R} = \left[E(r^2 + a^2) + L_z a\right]^2 - \Delta\left[m^2 r^2 + (L_z + aE)^2 + \mathcal{Q}\right]\,, \tag{64}$$

where λ is the affine parameter of the trajectory. The conserved quantity $\mathcal{Q}$ takes the explicit form $\mathcal{Q} = L^2 - L_z^2 - a^2(E^2 - m^2)\cos^2\theta_\infty$, where θ_∞ is the value of the azimuthal angle as the particle approaches the black hole from infinity, and L the total angular momentum of the particle.

A particle approaching a rotating black hole from infinity, may do so by following a number of possible trajectories. Here, we will be interested in the case of a massless particle with its trajectory being either transverse ($\theta_\infty = \pi/2$) or parallel ($\theta_\infty = 0, \pi$) to the rotation axis. Starting with the first case, we notice that, for motion strictly on the equatorial plane, $\cos\theta_\infty = 0$ and $L = L_z$. Then, $\mathcal{Q} = 0$, and Eq. (64) takes the form

$$\left(\Sigma \frac{dr}{d\lambda}\right)^2 = E^2\left[b^2(a^2 - \Delta) + 2b\,\frac{a\mu}{r^{n-1}} + (r^2 + a^2)^2 - a^2\Delta\right]. \tag{65}$$

In the above, we have defined $L/E \equiv b$, where $b > 0$ is the impact parameter of the particle. For the above equation to be consistent, its right-hand-side, or equivalently the expression inside the square brackets, must be positive-definite. Since the particle approaches the black hole from large r, we focus our attention on the radial regime outside the ergosphere, where the coefficient of b^2, $(a^2 - \Delta)$, can be shown to be negative. Then, the constraint on the values of b takes the form $b_2 < b < b_1$, where $b_{1,2}$ are the roots of the equation, following by setting the right-hand-side of Eq. (65) equal to zero. However, it may easily be seen that $b_2 < 0$, therefore, the classically acceptable regime is defined by the constraint $0 < b < b_1$. Particles with impact parameters in this regime can access all values of the radial coordinate, and thus reach the black-hole horizon, too, where they get absorbed. According to the geometrical optics argument, then, the closest distance the particle can get to the black hole without being captured is

$$r_c = \min(b_1) = \min\left(\frac{a\mu + r^{n+1}\sqrt{a^2 + r^2 - \frac{\mu}{r^{n-1}}}}{r^{n+1} - \mu}\right). \tag{66}$$

As a consistency check, we observe that, for $a = 0$, the above expression reduces to $r_c = \min\left(r/\sqrt{1 - \frac{\mu}{r^{n+1}}}\right)$, which leads directly to the result (63) for a non-rotating brane black-hole background derived in [44, 13]. By further setting $n = 0$, the purely 4-dimensional Schwarzschild case [40, 41, 42] is also recovered, with $r_c = 3\sqrt{3}\, r_h/2$.

For general n and a, an analytic expression for the minimum distance r_c is difficult to find. Nevertheless, a simple numerical analysis may lead to the value of r_c in units of r_h, after using Eq. (6) to eliminate the mass parameter μ from Eq. (66). Then, through

$\mathbf{a_*\backslash n}$	1	2	3	4	5	6
0.0	12.6	9.6	8.2	7.3	6.6	6.2
0.3	17.9	12.8	10.4	9.0	8.1	7.4
0.5	23.5	15.9	12.6	10.7	9.5	8.7
0.7	31.0	20.0	15.4	12.9	11.4	10.3
1.0	46.0	27.6	20.6	17.0	14.8	13.4
1.5	81.9	44.3	31.7	25.6	22.2	19.9
2.0	131.6	65.4	45.3	36.3	31.3	28.2

$\mathbf{a_*\backslash n}$	1	2	3	4	5	6
0.0	12.6	9.6	8.2	7.3	6.6	6.2
0.3	10.0	8.2	7.3	6.6	6.2	5.9
0.5	9.5	8.1	7.3	6.8	6.4	6.1
0.7	9.5	8.4	7.7	7.3	6.9	6.7
1.0	10.5	9.6	9.0	8.6	8.4	8.1
1.5	13.4	13.2	12.7	12.3	12.1	11.9
2.0	19.2	18.5	18.1	17.8	17.5	17.4

Table 2: Absorption cross-section $\sigma_{\rm abs}$ (in units of r_h^2) for particles moving in the equatorial plane of the axially-symmetric brane black hole (8), for $a > 0$ (upper sub-table) and $a < 0$ (lower sub-table).

the relation $\sigma_{\rm abs} = \pi r_c^2$, the corresponding absorption cross-section may be found; its values, for a variety of n and a_*, are displayed in Table 2. The two sub-tables correspond to the two possible orientations of the particle's angular momentum L: as it approaches the black hole from infinity moving in the equatorial plane, its angular momentum and the black-hole one can either be parallel ($aL > 0$) or anti-parallel ($aL < 0$). Here, we have assumed that $L > 0$ always, and considered two different choices for the sign of the angular momentum parameter of the black hole, $a > 0$ and $a < 0$, that correspond to the first and second sub-table of Table 2, respectively. For $a < 0$, the sign of the $a\mu$-term in the numerator of Eq. (66) is reversed, a modification that leads to a lower value of r_c and eventually of the cross-section.

We now proceed to the case of a zero-mass particle coming from infinity in an orbit parallel to the black hole's rotation axis. This translates into $\cos^2\theta_\infty = 1$ and $L_z = 0$. In that case, we find

$$\left(\Sigma\,\frac{dr}{d\lambda}\right)^2 = E^2(r^2+a^2)^2 - \Delta L^2. \tag{67}$$

Defining, as before, $b \equiv L/E$, one may easily conclude that the above equation is again consistent only if

$$b < \left(\frac{r^2+a^2}{\sqrt{\Delta}}\right). \tag{68}$$

The above leads to the minimum distance of the particle's approach to the black hole

$\mathbf{a_*\backslash n}$	1	2	3	4	5	6
0.0	12.6	9.6	8.2	7.3	6.6	6.2
0.3	13.7	10.4	8.7	7.8	7.1	6.6
0.5	15.7	11.6	9.7	8.6	7.9	7.3
0.7	18.7	13.5	11.2	9.8	9.0	8.4
1.0	25.1	17.2	14.0	12.3	11.3	10.5
1.5	40.9	25.7	20.5	18.0	16.5	15.4
2.0	62.8	36.5	28.9	25.3	23.3	22.0

Table 3: Absorption cross-section $\sigma_{\rm abs}$, in units of r_h^2, for particles moving parallel to the rotation axis of the axially-symmetric brane black hole (8).

without being captured given by

$$r_c = \min\left(\frac{r^2+a^2}{\sqrt{a^2+r^2-\frac{\mu}{r^{n-1}}}}\right) . \tag{69}$$

For $a=0$, the above result also reduces to the Schwarzschild-like one (63), as expected, since, in the absence of rotation, all directions of the particle's orbit should give the same result. By using Eq. (69), the values of the corresponding absorption cross-section $\sigma_{\rm abs}$, in units of r_h^2, are given in Table 3.

Let us now compare the various analytic values, obtained above by using the geometrical optics limit, with the numerical ones for the high-energy asymptotic value of the absorption cross-section. One should, of course, be careful when a direct comparison of these results is made: the values displayed in Tables 2 and 3 correspond to trajectories with a specific azimuthal angle, while the numerical values of Table 1 are actually integrated over all angles. Nevertheless, a comparison between the two sets of results could reveal, upon finding an agreement, which type of trajectories may be used to account for the value of the total cross-section more accurately. A direct comparison of the entries of Tables 1 and 2 shows that the total cross-section is smaller than the one corresponding to a trajectory lying on the equatorial plane with $aL>0$, but larger than the one with $aL<0$. On the other hand, by comparing the entries of Tables 1 and 3, we find that there is an almost perfect agreement between these two sets of results for low values of either a_* or n. The same agreement can be pictorially seen in Fig. 5, where the particular case $n=2$ and $a_*=0.3$ is shown. We may thus conclude that particle trajectories running parallel to the rotation axis of the black hole lead to an absorption cross-section whose value is virtually identical to the total one. As either n or a_* increases further, the two sets deviate; in this parameter regime, the contribution of all possible particle trajectories needs to be more carefully taken into account before the value of the total absorption cross-section can be justified.

5 Conclusions

The emission of Hawking radiation, i.e. the evaporation of a black hole via the emission of elementary particles, takes place during the *spin-down* and *Schwarzschild* phase of its life. Although the emission during the Schwarzschild phase of a higher-dimensional black hole was studied, both analytically and numerically, quite early, the complexity of the gravitational background around a similar, but rotating, black hole delayed the study of the spin-down phase. During the last few years, numerical studies have derived results for the various spectra characterising the emission of elementary particles on the brane by a higher-dimensional rotating black hole – the most phenomenologically interesting emission channel for the brane-localised observers. Nevertheless, no analytical studies have been performed and no analytic expressions for the fundamental quantities governing the emission of Hawking radiation, such as the absorption probability, have ever been derived for an arbitrary value of the number of extra dimensions n. In this work, we have duly performed this task, and studied in detail the properties of the absorption probability and absorption cross-section for scalar fields emitted on the brane by the $(4+n)$-dimensional axially-symmetric black hole.

As the complexity of the equation of motion, describing the propagation of a scalar field in the axially-symmetric brane background, forbids the derivation of a general solution for a particle with arbitrary frequency, we were forced to focus our analysis on two particular energy regimes: the low-energy one and the high-energy one. The low-energy regime was studied in Section 3, where an analytic solution for the radial part of the scalar-field wave-function was derived. This involved matching the near-horizon and far-field asymptotic solutions in an intermediate regime, and allowed calculation of the absorption probability. Our analytic results, formally valid only for low values of the energy parameter ωr_h and angular momentum parameter a_*, were compared with the exact numerical results, that were also reproduced during our analysis in an attempt to check the range of validity of our approximations. The two sets of results were found to be in excellent agreement in the low-energy regime, as expected. In addition, even for moderately large values of ωr_h and a_*, the agreement on both qualitative and quantitative levels still persisted.

The properties of the absorption probability in the low-energy regime, as these follow from our analytic results, were then studied in detail. Its dependence on the angular momentum numbers (l, m) was investigated first, with our analysis revealing the dominance of the lowest partial mode $l = 0$, and the one with $m = -|l|$, for fixed l. The absorption probability was also found to strongly depend on the spacetime topological parameters, namely the angular momentum parameter a_* of the black hole and the number of extra dimensions n: the non-superradiant modes with $m \leq 0$, were shown to be enhanced with both a_* and n, while the superradiant ones, with $m > 0$, were, on the contrary, suppressed – however, outside the superradiant regime, the latter modes were enhanced with n. Our analytic expression for the absorption probability, valid in the low-energy regime, was then expanded in the limit $\omega \to 0$, and the constant asymptotic value of the absorption cross-section was derived. The analytic value was shown to accurately reproduce, for small a_*, the exact numerical one, that was equal to the area of the horizon of the projected-on-the-brane axially-symmetric black hole, $4\pi(a^2 + r_h^2)$.

We subsequently turned our attention to the study of the scalar equation of motion in the high-energy regime. By using an analogous approximate method, and for the first time in the literature, an analytic solution was derived that perfectly matched the exact numerical one for large enough values of the energy parameter ωr_h. The value of ωr_h, beyond which the two solutions completely coincide, was shown to be strongly mode-dependent: modes with small l allowed the two solutions to match fairly quickly, while, modes with larger l had the matching taking place at an increasing value of the energy parameter. By employing the exact numerical solution for the absorption probability, valid at all energy regimes, we were able to determine the constant asymptotic value of the total absorption cross-section at the high-energy regime, and its dependence on n and a_*. Similarly to the spherically-symmetric case, this asymptotic value is suppressed as the number of extra dimensions increases. On the other hand, an increase in the angular momentum of the black hole causes an enhancement in the high-energy asymptotic value of $\sigma_{\rm abs}$. A detailed analysis, based on the geometrical optics limit, revealed that the asymptotic value of the absorption cross-section in the high-energy limit is accurately reproduced by considering particle trajectories approaching the black hole from infinity and running parallel to the rotation axis of the black hole.

The analytic results, supplemented by exact numerical ones, derived in this work, on the behaviour of the absorption probability and cross-section for scalar particles propagating in an axially-symmetric brane black-hole background, smoothly complement the sole previous analytic study of the 5-dimensional case [32], as well as the numerical studies of the Hawking radiation spectrum of [23, 25, 27]. Given the excellent agreement between our analytic solutions and the exact numerical ones, in the low and high-energy regime, their use to derive the corresponding emission rates would have led to results identical to the ones already presented in the works cited above. For that reason, we have refrained from performing this task here, and refer the interested reader to those works. Instead, in this manuscript, we have focused our attention on the derivation of closed-form expressions and study of the properties of the absorption probability and cross-section, that carry a significant amount of information on particle properties as well as on properties of the spacetime. Apart from their obvious theoretical interest, the above results may have a phenomenological one too: both our analytic solutions could be reliably used, in place of the exact numerical ones, to derive the energy emission rates in the low and high-energy regimes; these could then be used for the interpretation of any observable effects coming from an evaporating black hole produced in a ground-based accelerator and centered in these two frequency regimes. In the high-energy regime, in particular, where constraints on the available running time may put limits on the derivation of numerical data, our analytic solution may prove useful in removing the need for numerical integration.

Acknowledgments. We would like to thank C. Harris for providing the basis for our numerical code, and E. Winstanley for useful discussions in the early stages of this work. S.C and O.E. acknowledge PPARC and I.K.Y. fellowships, respectively. The work of P.K. is funded by the UK PPARC Research Grant PPA/A/S/ 2002/00350. P.K. and K.T. acknowledge participation in the RTN Universenet (MRTN-CT-2006035863-1). This research was co-funded by the European Union in the framework of the Program

$\Pi Y\Theta AI\Gamma OPA\Sigma - II$ of the *"Operational Program for Education and Initial Vocational Training"* ($E\Pi EAEK$) of the 3rd Community Support Framework of the Hellenic Ministry of Education, funded by 25% from national sources and by 75% from the European Social Fund (ESF).

References

[1] N. Arkani-Hamed, S. Dimopoulos and G. R. Dvali, *Phys. Lett.* B **429**, 263 (1998) [hep-ph/9803315]; *Phys. Rev.* D **59**, 086004 (1999) [hep-ph/9807344]; I. Antoniadis, N. Arkani-Hamed, S. Dimopoulos and G. R. Dvali, *Phys. Lett.* B **436**, 257 (1998) [hep-ph/9804398].

[2] L. Randall and R. Sundrum, *Phys. Rev. Lett.* **83** (1999) 3370 [hep-ph/9905221]; *Phys. Rev. Lett.* **83** (1999) 4690 [hep-ph/9906064].

[3] T. Banks and W. Fischler, hep-th/9906038;
D. M. Eardley and S. B. Giddings, *Phys. Rev.* **D66**, 044011 (2002) [gr-qc/0201034];
H. Yoshino and Y. Nambu, *Phys. Rev.* **D66**, 065004 (2002) [gr-qc/0204060];
Phys. Rev. **D67**, 024009 (2003) [gr-qc/0209003];
E. Kohlprath and G. Veneziano, *JHEP* **0206**, 057 (2002) [gr-qc/0203093];
V. Cardoso, O. J. C. Dias and J. P. S. Lemos, *Phys. Rev.* D **67**, 064026 (2003)[hep-th/0212168];
E. Berti, M. Cavaglia and L. Gualtieri, *Phys. Rev.* **D69**, 124011 (2004) [hep-th/ 0309203];
V. S. Rychkov, *Phys. Rev.* D **70**, 044003 (2004) [hep-ph/0401116];
S. B. Giddings and V. S. Rychkov, *Phys. Rev.* D **70**, 104026 (2004) [hep-th/0409131];
O. I. Vasilenko, hep-th/0305067;
H. Yoshino and V. S. Rychkov, *Phys. Rev.* D **71** (2005) 104028 [hep-th/0503171];
D. C. Dai, G. D. Starkman and D. Stojkovic, *Phys. Rev.* **73** (2006) 104037 [hep-ph/0605085];
H. Yoshino and R. B. Mann, *Phys. Rev.* **74** (2006) 044003 [gr-qc/0605131];
H. Yoshino, T. Shiromizu and M. Shibata, *Phys. Rev.* D **74**, 124022 (2006)[gr-qc/0610110].

[4] P. C. Argyres, S. Dimopoulos and J. March-Russell, *Phys. Lett.* B **441**, 96 (1998) [hep-th/9808138].

[5] P. Kanti, *Int. J. Mod. Phys.* A **19**, 4899 (2004) [hep-ph/0402168].

[6] S. B. Giddings and S. Thomas, *Phys. Rev.* D **65**, 056010 (2002) [hep-ph/0106219];
S. Dimopoulos and G. Landsberg, *Phys. Rev. Lett.* **87**, 161602 (2001) [hep-ph/0106295];
S. Dimopoulos and R. Emparan, *Phys. Lett.* B **526**, 393 (2002) [hep-ph/0108060];
S. Hossenfelder, S. Hofmann, M. Bleicher and H. Stocker, *Phys. Rev.* D **66**, 101502 (2002) [hep-ph/0109085];
K. Cheung, *Phys. Rev. Lett.* **88**, 221602 (2002) [hep-ph/0110163];

R. Casadio and B. Harms, *Int. J. Mod. Phys.* A **17**, 4635 (2002) [hep-th/0110255];
S. C. Park and H. S. Song, *J. Korean Phys. Soc.* **43**, 30 (2003) [hep-ph/0111069];
G. Landsberg, *Phys. Rev. Lett.* **88**, 181801 (2002) [hep-ph/0112061];
G. F. Giudice, R. Rattazzi and J. D. Wells, *Nucl. Phys.* B **630**, 293 (2002) [hep-ph/0112161];
E. J. Ahn, M. Cavaglia and A. V. Olinto, *Phys. Lett.* B **551**, 1 (2003)[hep-th/0201042];
T. G. Rizzo, *JHEP* **0202**, 011 (2002) [hep-ph/0201228]; *JHEP* **0501**, 028 (2005) [hep-ph/0412087]; hep-ph/0611224;
A. V. Kotwal and C. Hays, *Phys. Rev.* D **66**, 116005 (2002) [hep-ph/0206055];
A. Chamblin and G. C. Nayak, *Phys. Rev.* D **66**, 091901 (2002) [hep-ph/0206060];
T. Han, G. D. Kribs and B. McElrath, *Phys. Rev. Lett.* **90**, 031601 (2003) [hep-ph/0207003];
I. Mocioiu, Y. Nara and I. Sarcevic, *Phys. Lett.* B **557**, 87 (2003) [hep-ph/0301073];
M. Cavaglia, S. Das and R. Maartens, *Class. Quant. Grav.* **20**, L205 (2003) [hep-ph/0305223];
D. Stojkovic, *Phys. Rev. Lett.* **94**, 011603 (2005) [hep-ph/0409124];
S. Hossenfelder, *Mod. Phys. Lett.* A **19**, 2727 (2004) [hep-ph/0410122];
C. M. Harris, M. J. Palmer, M. A. Parker, P. Richardson, A. Sabetfakhri and B. R. Webber, *JHEP* **0505**, 053 (2005) [hep-ph/0411022];
G. C. Nayak and J. Smith, *Phys. Rev.* D **74**, 014007 (2006) [hep-ph/0602129];
H. Stocker, hep-ph/0605062;
L. Lonnblad and M. Sjodahl, *JHEP* **10** (2006) 088 [hep-ph/0608210];
M. Cavaglia, R. Godang, L. Cremaldi and D. Summers, hep-ph/0609001;
G. L. Alberghi, R. Casadio and A. Tronconi, hep-ph/0611009.

[7] A. Goyal, A. Gupta and N. Mahajan, *Phys. Rev.* D **63**, 043003 (2001) [hep-ph/0005030];
J. L. Feng and A. D. Shapere, *Phys. Rev. Lett.* **88**, 021303 (2001) [hep-ph/0109106];
L. Anchordoqui and H. Goldberg, *Phys. Rev.* D **65**, 047502 (2002) [hep-ph/0109-242];
R. Emparan, M. Masip and R. Rattazzi, *Phys. Rev.* D **65**, 064023 (2002) [hep-ph/ 0109287];
L. A. Anchordoqui, J. L. Feng, H. Goldberg and A. D. Shapere, *Phys. Rev.* D **65**, 124027 (2002) [hep-ph/0112247]; *Phys. Rev.* D **68**, 104025 (2003) [hep-ph/0307228];
Y. Uehara, *Prog. Theor. Phys.* **107**, 621 (2002) [hep-ph/0110382];
J. Alvarez-Muniz, J. L. Feng, F. Halzen, T. Han and D. Hooper, *Phys. Rev.* D **65**, 124015 (2002) [hep-ph/0202081];
A. Ringwald and H. Tu, *Phys. Lett.* B **525**, 135 (2002) [hep-ph/0111042];
M. Kowalski, A. Ringwald and H. Tu, *Phys. Lett.* B **529**, 1 (2002) [hep-ph/0111042];
E. J. Ahn, M. Ave, M. Cavaglia and A. V. Olinto, *Phys. Rev.* D **68**, 043004 (2003) [hep-ph/0306008];
A. Mironov, A. Morozov and T. N. Tomaras, hep-ph/0311318;
E. J. Ahn, M. Cavaglia and A. V. Olinto, *Astropart. Phys.* **22**, 377 (2005) [hep-ph/0312249];
T. Han and D. Hooper, *New J. Phys.* **6** (2004) 150 [hep-ph/0408348];

A. Cafarella, C. Coriano and T. N. Tomaras, *JHEP* **0506**, 065 (2005) [hep-ph/0410358];
D. Stojkovic and G. D. Starkman, *Phys. Rev. Lett.* **96**, 041303 (2006) [hep-ph/0505112];
A. Barrau, C. Feron and J. Grain, *Astrophys. J.* **630**, 1015 (2005) [astro-ph/0505436];
L. Anchordoqui, T. Han, D. Hooper and S. Sarkar, *Astropart. Phys.* **25**, 14 (2006) [hep-ph/0508312];
E. J. Ahn and M. Cavaglia, *Phys. Rev.* D **73**, 042002 (2006) [hep-ph/0511159];
L. A. Anchordoqui, M. M. Glenz and L. Parker, *Phys. Rev.* D **75**, 024011 (2007) [hep-ph/0610359].

[8] M. Cavaglia, *Int. J. Mod. Phys.* **A18**, 1843 (2003) [hep-ph/0210296]; G. Landsberg, *Eur. Phys. J.* **C33**, S927 (2004) [hep-ex/0310034]; K. Cheung, hep-ph/0409028; S. Hossenfelder, hep-ph/0412265; A. S. Majumdar and N. Mukherjee, *Int. J. Mod. Phys.* D **14**, 1095 (2005) [astro-ph/0503473]; A. Casanova and E. Spallucci, *Class. Quant. Grav.* **23**, R45 (2006) [hep-ph/0512063].

[9] C. M. Harris, hep-ph/0502005.

[10] S. W. Hawking, *Commun. Math. Phys.* **43**, 199 (1975).

[11] P. Kanti and J. March-Russell, *Phys. Rev.* D **66**, 024023 (2002) [hep-ph/0203223]; *Phys. Rev.* D **67**, 104019 (2003) [hep-ph/0212199].

[12] V. P. Frolov and D. Stojkovic, *Phys. Rev.* D **66**, 084002 (2002) [hep-th/0206046]; *Phys. Rev.* D **67**, 084004 (2003) [gr-qc/0211055].

[13] C. M. Harris and P. Kanti, *JHEP* **0310**, 014 (2003) [hep-ph/0309054].

[14] P. Kanti, J. Grain and A. Barrau, *Phys. Rev.* D **71** (2005) 104002 [hep-th/0501148].

[15] A. Barrau, J. Grain and S. O. Alexeyev, *Phys. Lett.* B **584**, 114 (2004) [hep-ph/0311238]; J. Grain, A. Barrau and P. Kanti, *Phys. Rev.* D **72**, 104016 (2005) [hep-th/0509128]; T. G. Rizzo, *Class. Quant. Grav.* **23**, 4263 (2006) [hep-ph/0601-029]; hep-ph/0603242.

[16] E. l. Jung, S. H. Kim and D. K. Park, *Phys. Lett.* B **586** (2004) 390 [hep-th/0311036]; *JHEP* **0409** (2004) 005 [hep-th/0406117]; *Phys. Lett.* B **602** (2004) 105 [hep-th/0409145]; *Phys. Lett.* B **614** (2005) 78 [hep-th/0503027]; E. Jung and D. K. Park, *Nucl. Phys.* B **717** (2005) 272 [hep-th/0502002]; hep-th/0506204.

[17] D. C. Dai, N. Kaloper, G. D. Starkman and D. Stojkovic, hep-th/0611184.

[18] L. Liu, B. Wang and G. Yang, hep-th/0701166.

[19] A. S. Cornell, W. Naylor and M. Sasaki, *JHEP* **0602** (2006) 012 [hep-th/0510009].

[20] D. K. Park, *Class. Quant. Grav.* **23** (2006) 4101 [hep-th/0512021].

[21] V. Cardoso, M. Cavaglia and L. Gualtieri, *Phys. Rev. Lett.* **96**, 071301 (2006) [Erratum-ibid. **96**, 219902 (2006)] [hep-th/0512002]; *JHEP* **0602**, 021 (2006) [hep-th/0512116].

[22] S. Creek, O. Efthimiou, P. Kanti and K. Tamvakis, *Phys. Lett.* B **635** (2006) 39 [hep-th/0601126]; O. Efthimiou, hep-th/0609144.

[23] C. M. Harris and P. Kanti, *Phys. Lett.* B **633**, 106 (2006) [hep-th/0503010].

[24] D. Ida, K. y. Oda and S. C. Park, hep-ph/0501210.

[25] G. Duffy, C. Harris, P. Kanti and E. Winstanley, *JHEP* **0509**, 049 (2005) [hep-th/0507274].

[26] M. Casals, P. Kanti and E. Winstanley, *JHEP* **0602**, 051 (2006) [hep-th/0511163]; M. Casals, S. R. Dolan, P. Kanti and E. Winstanley, hep-th/0608193.

[27] D. Ida, K. y. Oda and S. C. Park, *Phys. Rev.* D **71**, 124039 (2005) [hep-th/0503052]; *Phys. Rev.* D **73**, 124022 (2006) [hep-th/0602188].

[28] E. Jung, S. Kim and D. K. Park, *Phys. Lett.* B **615**, 273 (2005) [hep-th/0503163]; *Phys. Lett.* B **619**, 347 (2005) [hep-th/0504139].

[29] H. Nomura, S. Yoshida, M. Tanabe and K. i. Maeda, *Prog. Theor. Phys.* **114**, 707 (2005) [hep-th/0502179].

[30] E. Jung and D. K. Park, *Nucl. Phys.* B **731**, 171 (2005) [hep-th/0506204].

[31] V. P. Frolov and D. Stojkovic, *Phys. Rev.* D **67**, 084004 (2003) [gr-qc/0211055].

[32] D. Ida, K. y. Oda and S. C. Park, *Phys. Rev.* D **67**, 064025 (2003) [Erratum-ibid. D **69**, 049901 (2004)] [hep-th/0212108].

[33] R. C. Myers and M. J. Perry, *Annals Phys.* **172**, 304 (1986).

[34] C. Flammer, *Spheroidal wave functions* (Stanford University Press, 1957);
J. N. Goldberg, A. J. MacFarlane, E. T. Newman, F. Rohrlich and E. C. Sudarshan, *J. Math. Phys.* **8**, 2155 (1967);
J. Meixner, F. W. Schäfke, and G. Wolf, *Mathieu functions and spheroidal functions and their mathematical foundations, further studies* (Springer-Verlag, Berlin, 1980).

[35] A. A. Starobinskii and S. M. Churilov, *Sov. Phys.-JETP* **38**, 1 (1974);
E. D. Fackerell and R. G. Crossman, *J. Math. Phys.* **18**, 1849 (1977);
E. Seidel, *Class. Quant. Grav.* **6**, 1057 (1989).

[36] M. Abramowitz and I. Stegun, *Handbook of Mathematical Functions* (Academic, New York, 1996).

[37] S. Chandrasekhar, *The Mathematical Theory of Black Holes* (Oxford University Press, New York, 1983).

[38] Y.B. Zel'dovich, *JETP Lett.* **14**, 180 (1971).

[39] S. S. Gubser, I. R. Klebanov and A. A. Tseytlin, *Nucl. Phys.* **B499**, 217 (1997) [hep-th/9703040];
S. D. Mathur, *Nucl. Phys. B* **514**, 204 (1998) [hep-th/9704156];
S. S. Gubser, *Phys. Rev. D* **56**, 4984 (1997) [hep-th/9704195].

[40] C. W. Misner, K. S. Thorne and J. A. Wheeler, *Gravitation* (W.H. Freeman & Cp., New York, 1973).

[41] D. N. Page, *Phys. Rev.* D **13** (1976) 198.

[42] N. G. Sanchez, *Phys. Rev.* D **16** (1977) 937; *Phys. Rev.* D **18** (1978) 1030; *Phys. Rev.* D **18** (1978) 1798.

[43] J. H. MacGibbon and B. R. Webber, *Phys. Rev.* D **41**, 3052 (1990).

[44] R. Emparan, G. T. Horowitz and R. C. Myers, *Phys. Rev. Lett.* **85**, 499 (2000) [hep-th/0003118].

[45] V. P. Frolov and I. D. Novikov, *Black hole physics: Basic concepts and new developments* (Kluwer Academic, Dordrecht, Netherlands, 1998).